

Analysis of the ionic and dielectric properties of perovskites by impedance spectroscopy

Cite as: J. Appl. Phys. **133**, 045501 (2023); <https://doi.org/10.1063/5.0123547>

Submitted: 31 August 2022 • Accepted: 06 January 2023 • Published Online: 24 January 2023

 Cong Xu,  Mohammad Sajedi Alvar,  Gert-Jan A. H. Wetzelaer, et al.



View Online



Export Citation



CrossMark

ARTICLES YOU MAY BE INTERESTED IN

[Tutorial: Lead sulfide colloidal quantum dot infrared photodetector](#)

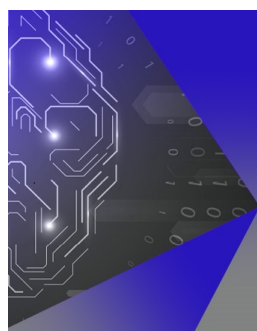
Journal of Applied Physics **133**, 041101 (2023); <https://doi.org/10.1063/5.0133809>

[Emerging multi-frequency surface strain force microscopy](#)

Journal of Applied Physics **133**, 040901 (2023); <https://doi.org/10.1063/5.0131075>

[Epitaxial synthesis of unintentionally doped p-type SnO \(001\) via suboxide molecular beam epitaxy](#)

Journal of Applied Physics **133**, 045701 (2023); <https://doi.org/10.1063/5.0131138>



APL Machine Learning

Machine Learning for Applied Physics
Applied Physics for Machine Learning

**First Articles
Now Online!**

Analysis of the ionic and dielectric properties of perovskites by impedance spectroscopy

Cite as: J. Appl. Phys. 133, 045501 (2023); doi: 10.1063/5.0123547

Submitted: 31 August 2022 · Accepted: 6 January 2023 ·

Published Online: 24 January 2023





View Online



Export Citation



CrossMark

Cong Xu,  Mohammad Sajedi Alvar,  Cert-Jan A. H. Wetzelaer,  and Paul W. M. Blom^{a)} 

AFFILIATIONS

Max Planck Institute for Polymer Research, Ackermannweg 10, 55128 Mainz, Germany

^{a)}Author to whom correspondence should be addressed: blom@mpip-mainz.mpg.de

ABSTRACT

For understanding the operation of perovskite solar cells and light-emitting diodes, knowledge of the dielectric properties is indispensable. The dielectric properties of perovskites are frequency dependent due to the presence of moving ions, which complicates the interpretation of impedance spectra. Using Au/CsPbI₂Br/Au capacitors with varied layer thickness as a model system, we demonstrate that in the dark, an extended Maxwell circuit consistently describes the impedance data. From the thickness dependence of the resistivities, both the electronic and ionic conductivities are obtained, whereas the combination of electronic and ionic capacitances with the characteristic frequencies for space-charge formation determines the ion diffusion coefficient and ion density. At low frequencies, a slow transient process with a fixed time constant of ~ 0.1 s occurs, governed by the electronic conductivity, being independent of illumination strength and sample thickness. As a possible mechanism, we propose the spatial reorganization of ions within the ion accumulation layer at the electrode/perovskite interface.

© 2023 Author(s). All article content, except where otherwise noted, is licensed under a Creative Commons Attribution (CC BY) license (<http://creativecommons.org/licenses/by/4.0/>). <https://doi.org/10.1063/5.0123547>

I. INTRODUCTION

Hybrid organic–inorganic lead halide perovskites have emerged as a promising material for opto-electronic devices, such as solar cells¹ and light-emitting diodes.² Despite the impressive progress in efficiency, understanding of the device physics is still in early development. A complication in the analysis of electrical data is the occurrence of hysteresis due to slow moving ions.^{3–5} Upon the application of an electric field, ions move toward the biased electrode, thereby altering the charge injection properties as well as screening the electric field in the rest of the device. The amount of screening depends on the ion concentration and their ability to follow the applied field. As a result, the dielectric properties of perovskites are frequency dependent, which, in device modeling, can be incorporated as an effective dielectric constant.⁶ Impedance spectroscopy is a powerful technique to study such dynamical processes, since it is able to differentiate between processes that are relevant on different time scales.⁷ Typically, impedance spectra are analyzed using equivalent circuits, consisting of resistors and capacitors. The obtained magnitudes of these passive elements then provide information about the microscopic physical processes occurring in the device under test. A challenge for this approach to

be useful is the validation of the equivalent circuit used. For perovskite-based devices, it appeared that the interpretation of impedance spectra is not straightforward. In the dark, it was noted that the impedance spectra of the workhorse material methylammonium lead iodide (MAPbI₃) using Au/MAPbI₃/Au capacitors resemble those of electrolytes.⁸ For an electrolyte containing mobile positive ions sandwiched between blocking contacts, meaning that the ions cannot penetrate the electrodes, the application of an electrical signal with frequency f (or angular frequency $\omega = 2\pi f$) will move positive ions toward the negatively biased electrode, leaving fixed negatively charge ions behind. The accumulated positive ions at the electrode behave as an additional capacitor C_b , in series with a parallel RC-circuit, where C and R represent the capacitance and resistance of the bulk, respectively ($C_b \gg C$). One difference with regard to an electrolyte is that in a perovskite capacitor also, an electrical current can flow. For this reason, the equivalent circuit of the electrolyte was expanded with an additional parallel resistor R_i . As shown in Fig. 1(a), such an interfacial resistance R_i can then be regarded as a contact resistance for a device of which the electrical current is contact-limited. Using a theoretical model derived for electrolytes,⁹ the ion diffusion coefficient and ion concentration

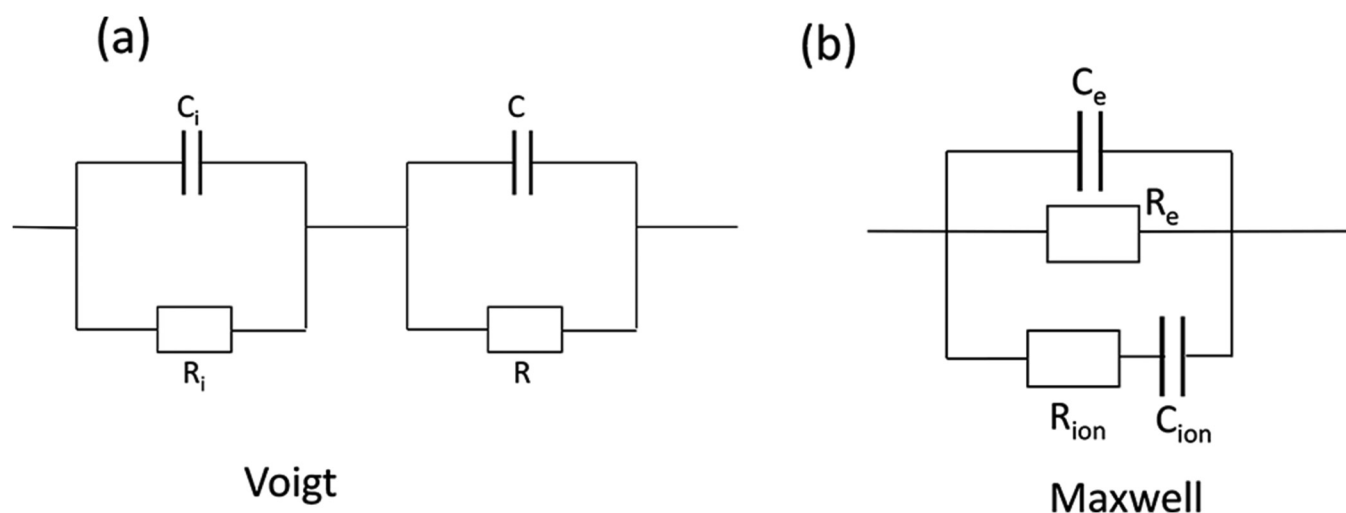


FIG. 1. Equivalent circuits used for perovskite capacitors including (a) two Voigt elements in series and (b) Maxwell elements.

could be extracted from characteristic frequencies in the impedance spectra.

Alternatively, an equivalent circuit, also known as the Maxwell circuit, was proposed for MAPbI₃ thin films taking into account ion migration, as shown in Fig. 1(b).¹⁰ In this circuit, the application of voltage leads to the polarization of the dielectric via C_e and also to the accumulation of ions at the interface via C_{ion} . The speed of ionic charging is governed by R_{ion} , whereas the resistance R_e due to an electronic current is in parallel to the ionic channel. However, we note that it can be shown that both circuits can give an identical frequency dependence of Z' and Z'' and that their parameters are similar and directly related (Sec. S1 in the [supplementary material](#)).⁷ As a result, from the dark impedance data, it cannot be discriminated which circuit, Voigt or Maxwell, is more appropriate for perovskite capacitors.

Upon the illumination of perovskite solar cells, a giant increase in the capacitance has been observed.¹¹ Several explanations for this phenomenon have been proposed, ranging from a giant dielectric constant related to ferroelectricity,¹¹ ion accumulation,¹² and surface charges.¹³ Furthermore, next to the giant capacitance also, a negative capacitance was observed under illumination.¹⁴ Such an inductive effect cannot be interpreted in terms of the accumulation of charges. In recent work, the occurrence of high capacitances under illumination at low frequencies has been attributed to transient currents that are delayed with regard to the applied voltage, termed as the ionic-to-electronic current amplification model.^{15–18} Upon illumination, the ions accumulating at the biased electrode due to the built-in electric field in a solar cell can modify the extraction of photogenerated charge carriers, giving rise to an increase or decrease in photocurrent.¹⁸ As demonstrated by Tress *et al.*, the gradient of the transient current then determines whether the observed apparent capacitance is positive or negative.¹⁷ The impedance response due to the transient current is represented by an RC element of which the RC time is a

constant, independent of voltage or light intensity, with a typical value of 0.1 s.¹⁷ Since the current transient is of electrical origin, the resistance of the RC element representing its impedance response is given by the electrical resistance R_e , which is dependent on voltage and light intensity, whereas the apparent transient capacitance C_{tr} equals the fixed time constant of the transient effect divided by R_e .¹⁷

One fundamental question that remains is whether transient effects also affect the low frequency impedance data of perovskite capacitors in the dark and how far this affects their interpretation in terms of ion dynamics, more specifically the ion concentration and diffusion coefficient. The ion migration under illumination and bias, as well as the volatility of an organic cation as methylammonium, makes MAPbI₃ less suited as a model material to disentangle the various contributions to the impedance. All-inorganic perovskites such as CsPbI₃ are thermally more stable and also exhibit improved photostability. Furthermore, it was found that ion migration in all-inorganic perovskites was less prominent as compared to hybrid compounds like MAPbI₃,¹⁹ and the power efficiency of solar cells based on all-inorganic solar cells now exceeds 20%.²⁰ Therefore, we study Au/CsPbI₂Br/Au capacitors as a function of CsPbI₂Br thickness to disentangle the various contributions to the impedance and validate the obtained ion dynamics. We demonstrate that the impedance spectra of Au/CsPbI₂Br/Au capacitors are consistently described by a Maxwell element with the common branch of a resistor and a capacitor in series representing the charging of ions at the electrode, extended with a second branch representing the transient current effect [inset in Fig. 2(a)]. The observed correlation between the obtained characteristic frequencies and capacitances validates the extraction of the ion concentration and diffusion coefficient from the dark impedance data. The impedance under illumination is governed by the strongly reduced electrical resistance that overrules the ion dynamics.

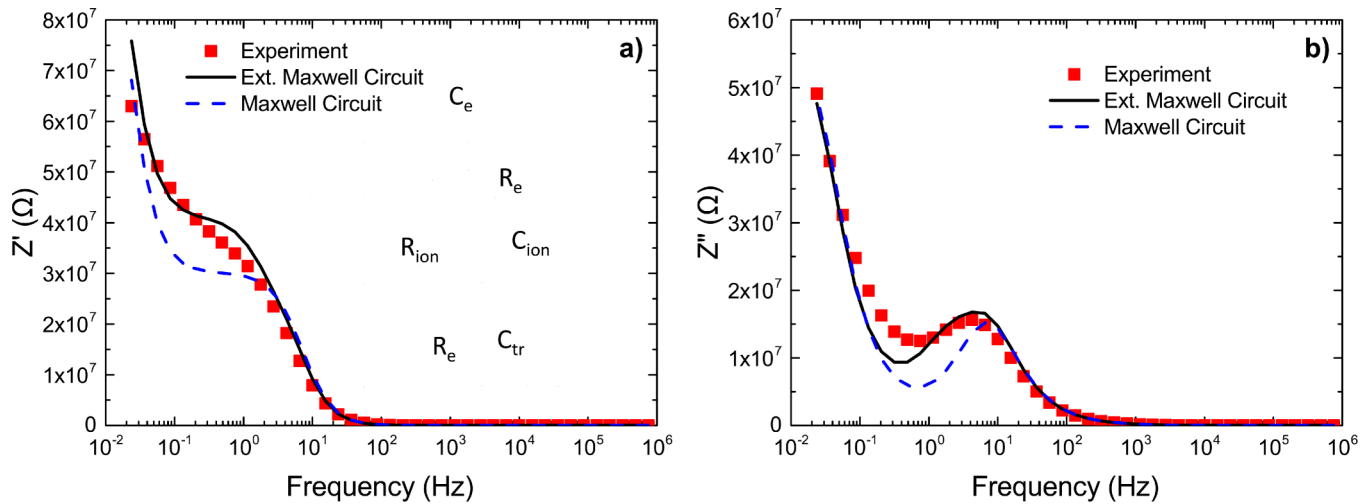


FIG. 2. (a) Real Z' and (b) imaginary Z'' part of the impedance Z (symbols) as a function of frequency f for an Au/CsPbI₂Br/Au capacitor with a thickness of 130 nm. The solid lines are a fit with the circuit shown in the inset in (a) using $R_e = 1.4 \times 10^8 \Omega$, $C_e = 7.5 \times 10^{-10} \text{ F}$, $R_{ion} = 6 \times 10^7 \Omega$, $C_{ion} = 4 \times 10^{-8} \text{ F}$, and $C_{tr} = 4 \times 10^{-10} \text{ F}$. The bulk capacitance C_e corresponds to a (high frequency) dielectric constant ϵ_r of 11. The dashed lines represent the fit where the transient branch is omitted.

II. RESULTS AND DISCUSSION

As a first step, the impedance data of a series of Au/CsPbI₂Br/Au capacitors with varying thickness are investigated in the dark. As an example, the real part of the impedance Z' and the imaginary part Z'' are shown as a function of frequency in Fig. 2. Also shown (lines) are the fits using the equivalent circuit shown in the inset in Fig. 2(a), representing the Maxwell circuit used to analyze MAPbI₃ capacitors¹⁰ but now extended with a second $R_e C_{tr}$ branch representing the transient current effect [inset in Fig. 2(a)] with parameters $R_e = 1.4 \times 10^8 \Omega$, $C_e = 7.5 \times 10^{-10} \text{ F}$, $R_{ion} = 6 \times 10^7 \Omega$, $C_{ion} = 4 \times 10^{-8} \text{ F}$, and $C_{tr} = 4 \times 10^{-10} \text{ F}$.

For the Maxwell circuit [Fig. 1(b)], the frequency (f_2) where the minimum in Z'' occurs [Fig. 2(b), dashed line] can be estimated from the values of the fitted circuit elements (Sec. S2 in the supplementary material). When using the extended Maxwell circuit including the $R_e C_{tr}$ branch to fit the impedance data, we note that this introduces one additional parameter C_{tr} , since the transient effect scales with the electrical resistance R_e .¹⁷ Using light intensity dependent measurements, we will also verify that the resistance in this additional transient branch is indeed governed by the electrical resistance R_e . To validate the application of this extended Maxwell circuit to the impedance data of perovskite capacitors, we have investigated a series of Au/CsPbI₂Br/Au capacitors with varying thickness d . In Table I, the obtained fit parameters are listed.

A subset of the experimental data and fits are also graphically represented in the Nyquist plots shown in Fig. 3. Similar to Fig. 2, there is good agreement between measurements and fits.

To give an indication of the accuracy of the obtained values for the circuit elements, we have also performed a statistical analysis, showing a relative error margin of the fits in between 5 and 15% (Sec. S3 in the supplementary material). Furthermore, the effect of a variation in R_e on the Z'' - f dependence has also been

included (Fig. S1 in the supplementary material), showing that a large variation of 30% also has a large effect on the calculated impedance. As expected, the geometrical bulk capacitance C_e scales with d^{-1} , and the resulting scaling corresponds to a (high frequency) dielectric constant ϵ_r of 11, which is in line with the earlier results.²¹ In contrast, the capacitance of the ionic interface layer is nearly thickness independent. Furthermore, the electrical resistance (R_e) and ionic resistance (R_{ion}) exhibit a linear dependence on thickness d , as shown in Fig. 4.

From the slope of the resistance vs thickness, characterized by $R = \sigma^{-1} d/A$, with A being the device area of 10^{-6} m^2 , the electrical conductivity σ_e and ionic conductivity σ_{ion} can be obtained. We find $\sigma_e = 1 \times 10^{-9} \text{ S/m}$ and $\sigma_{ion} = 2.5 \times 10^{-9} \text{ S/m}$, showing that in these capacitors, the resistance is mainly governed by the ionic conductivity. The large electrical resistance R_e is the result of the blocking nature of the Au/CsPbI₂Br contact. We note that the presence of such a large injection barrier strongly lowers the dark current, but not necessarily the extraction of carriers under illumination, since extraction is energetically a downhill process at the contact. This is evidenced by the strong decrease in R_e under illumination as shown later (Fig. 6). A consistency check is to analyze the imaginary part of the dielectric constant ϵ_r'' obtained from the impedance data, which according to Jonscher's law²² scales with $1/f$ according to $\epsilon_r'' = \sigma \epsilon_0^{-1} \omega^{-1}$, with $\omega = 2\pi f$. In Fig. 5(a), ϵ_r'' is shown as a function of $1/f$ for an Au/CsPbI₂Br/Au capacitor with a thickness of 600 nm. The slope shows a $1/f$ behavior in the frequency range of 10^{-2} – 10^2 Hz giving rise to $\sigma_{ion} = 2.9 \times 10^{-9} \text{ S/m}$, which is nearly equal to σ_{ion} obtained from the thickness dependence of the ionic resistance [Fig. 4(b)].

Having established that the low frequency part of the impedance is governed by the ionic conductivity, we can now analyze the ion dynamics. Recently, it has been noted that the impedance data

TABLE I. Values of circuit elements [inset of Fig. 1(a)] obtained from fitting Z' and Z'' for Au/CsPbI₂Br/Au capacitors with varying thickness as well as frequencies of the maximum (f_1) and minimum (f_2) in Z'' .

d (nm)	R_e (Ω)	C_e (F)	R_{ion} (Ω)	C_{ion} (F)	C_{tr}	f_1 (Hz)	f_2 (Hz)
130	1.4×10^8	7.5×10^{-10}	6.0×10^7	4.0×10^{-8}	4.5×10^{-10}	4.2	0.75
150	1.0×10^8	6.5×10^{-10}	6.0×10^7	4.0×10^{-8}	3.0×10^{-10}	4.2	0.48
170	1.3×10^8	5.8×10^{-10}	6.0×10^7	4.0×10^{-8}	4.0×10^{-10}	4.2	0.6
200	1.6×10^8	5.0×10^{-10}	8.0×10^7	3.0×10^{-8}	3.0×10^{-10}	4.2	0.48
250	2.0×10^8	4.0×10^{-10}	1.5×10^8	4.0×10^{-8}	4.0×10^{-10}	4.2	0.39
350	2.2×10^8	2.8×10^{-10}	8.5×10^7	3.0×10^{-8}	3.0×10^{-10}	5.3	0.48
400	7.0×10^8	2.4×10^{-10}	3.0×10^8	3.5×10^{-8}	1.5×10^{-10}	1.78	0.13
500	8.0×10^8	2.0×10^{-10}	3.0×10^8	3.0×10^{-8}	1.0×10^{-10}	1.15	0.08
600	6.0×10^8	1.7×10^{-10}	2.5×10^8	3.5×10^{-8}	1.2×10^{-10}	3.5	0.2
700	7.0×10^8	1.4×10^{-10}	3.0×10^8	4.0×10^{-8}	1.0×10^{-10}	2.73	0.2
1100	1.1×10^9	9.0×10^{-11}	6.0×10^8	3.0×10^{-8}	6.0×10^{-10}	2.73	0.13
2000	2.0×10^9	5.0×10^{-11}	1.0×10^9	3.0×10^{-8}	2.0×10^{-10}	1.78	0.08

of an Au/ MAPbI₃/Au capacitor look very similar to those of an electrolyte,⁸ which enabled the extraction of the ion diffusion coefficient and ion concentration from characteristic frequencies in the impedance spectra. For an electrolyte, the imaginary part of the impedance Z'' exhibits a maximum at angular frequency $\omega_1 = 1/\tau_1$ and a minimum at $\omega_2 = 1/\tau_2$.⁹ This maximum and minimum, thus, provides us with two characteristic time constants, representing the relaxation of the space-charge in the bulk and interface, τ_1 and τ_2 , respectively, which are related via

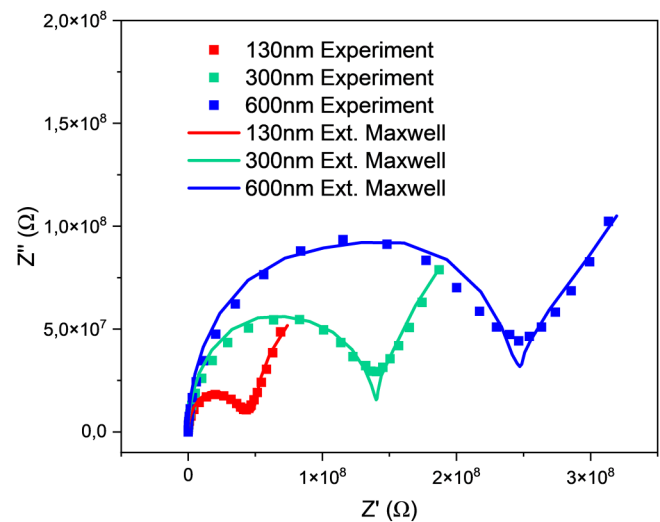
$$\tau_2 = \tau_1 \sqrt{\delta}, \quad (1)$$

with δ being defined as $C_{ion}/C_e = d/\lambda$, where λ is the Debye length. The Debye length is equal to $\sqrt{D_{ion}\tau_2}$, with D_{ion} being the ion diffusion coefficient. As a result, with τ_1 and τ_2 known, the ion diffusion coefficient D_{ion} is then directly given by

$$D_{ion} = \frac{L^2}{\tau_2 \delta^2}. \quad (2)$$

As a result, the obtained frequencies for the maximum and minimum (Table I), representing the built-up of ionic space charge, are quantitatively related to the proportion between the ionic and electrical capacitance. We note that 10^{-2} – 10^2 Hz is also the relevant frequency range where the maximum and minimum frequencies f_1 and f_2 occur. An important consistency check to validate that the obtained frequencies/time constants are indeed representing the formation of an ionic space charge layer at the contact is to compare the parameter δ obtained from the observed time constants [Eq. (1)] and from C_{ion}/C_e (Table I). Figure 5(b) shows δ as the function of layer thickness. It is demonstrated that the δ values from the characteristic time constants (blue symbols) agree well with the ratio of the capacitances (orange symbols). Furthermore, δ as expected from C_{ion}/C_e using $C_{ion} = 3.5 \times 10^{-8}$ F and $C_e = \epsilon_0 \epsilon_r A/d$ with $\epsilon_r = 11$ is indicated by the solid line. The agreement demonstrates that this model can, indeed, be applied to perovskite capacitors, under the condition that the ionic conductivity dominates the low frequency impedance. Using the

obtained values for δ , we obtain the diffusion coefficient $D_{ion} = 2 \times 10^{-17}$ m²/s. With the ion diffusion coefficient D_{ion} and, thus, ion mobility μ known via the Nernst-Einstein relation ($\mu = eD/kT$), knowledge of the ion conductivity σ_{ion} then directly gives the ion concentration $N_{ion} = \sigma_{ion}/e\mu$. Using $\sigma_{ion} = 2.5 \times 10^{-9}$ S/m, we obtain for the ion density $N_{ion} = 2 \times 10^{25}$ m⁻³. Compared to MAPbI₃, the diffusion coefficient is two orders of magnitude slower and the ion concentration is nearly equal. This confirms the earlier observations that in all-inorganic perovskites, ion migration is less prominent since the ions move very slowly.²⁰ With the ionic parameters known, also the frequency dependence of the effective dielectric constant ϵ_r' of CsPbI₂Br can be predicted using the

**FIG. 3.** Real Z' vs imaginary Z'' as a function of frequency f for Au/CsPbI₂Br/Au capacitors with a thickness of 130, 300, and 600 nm. The solid lines are a fit with the circuit shown in the inset in Fig. 2(a).

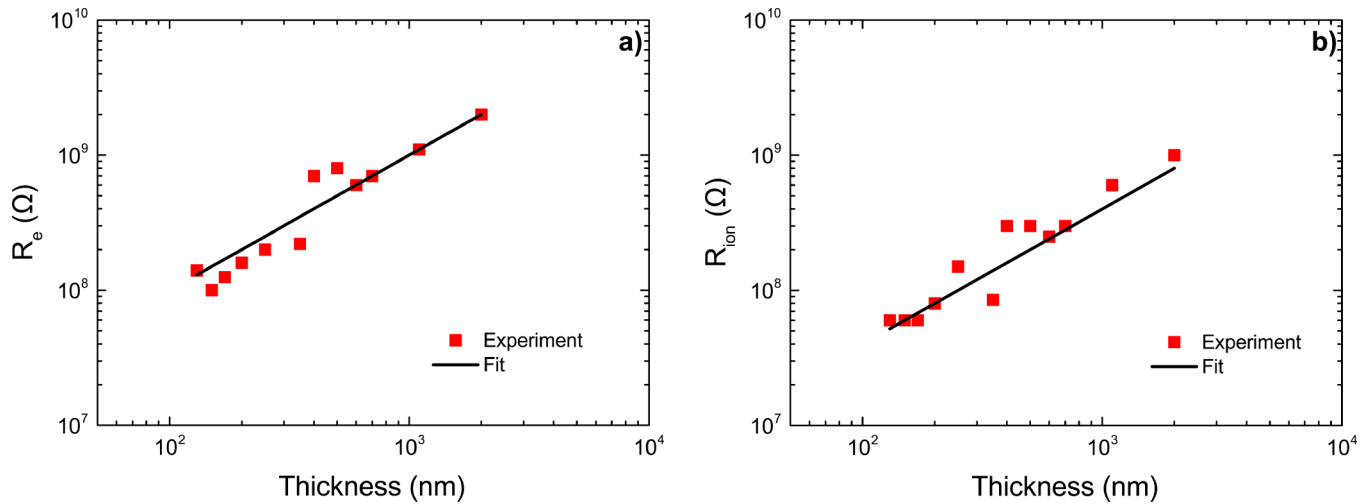


FIG. 4. (a) Electrical (R_e) and (b) ionic resistance (R_{ion}) as a function of thickness d of the CsPbI₂Br layer in Au/CsPbI₂Br/Au capacitors. The solid lines are calculated using $\sigma_e = 1 \times 10^{-9}$ S/m and $\sigma_{ion} = 2.5 \times 10^{-9}$ S/m.

model of Bandara and Mellander,⁹ given by

$$\epsilon_r' = \epsilon_\infty' \left(1 + \frac{\delta}{1 + (\omega\tau_1\delta)^2} \right). \quad (3)$$

In Fig. 5(c), the calculated effective dielectric constant ϵ_r' vs frequency [Eq. (3)] is shown (line), together with the measured epsilon ϵ_r' (symbols) obtained from

$$\epsilon' = \frac{-Z''}{\omega C_0(Z'^2 + Z''^2)}. \quad (4)$$

The model qualitatively describes the increase in the dielectric constant at low frequencies due to the ionic polarization, although it rises more steeply as compared to the experiment. It should be noted that in the model, all ions have the same mobility, and a slight dispersion in the ion mobility values would smoothen this increase at low frequencies.

So far, we have not paid attention to the branch representing the current transient effect. From the obtained values for R_e and C_{tr} , we obtain a thickness independent time constant $R_e C_{tr}$ of ~ 0.1 s. This is very similar to the value reported by Tress *et al.*¹⁷ However, we observe that also without this branch, a reasonably good fit can be made with nearly identical values for R_e , C_e , R_{ion2} and C_{ion} (Fig. 2, dotted lines). This shows that the influence of the transient process in the dark is not dominating the impedance due to the large values of R_{ion} and R_e that play a dominating role at low frequencies. However, an important observation is that the product $R_e \times C_{tr}$ is *thickness independent*, even when the thickness is varied over a large range of 130–2000 nm.

As a final step, we need to verify that the transient process is indeed governed by the electrical resistance R_e or, in other words, showing that the incorporation of R_e in the transient branch is

correct. For this purpose, we illuminate the Au/CsPbI₂Br/Au capacitors, which have a semi-transparent Au contact with a thickness of 18 nm on one side. It is expected that due to photoconduction, the electrical resistance R_e will strongly decrease, whereas the ionic resistance might not be affected. In Fig. 6, it is demonstrated how Z' (a) and Z'' (b) vary as the function of the illumination intensity I , given in the arbitrary units of 1, 5, 10, 25, and 50. Here, an illumination intensity of 100 corresponds to 1 Sun. For this purpose, Z' is multiplied with the light intensity I , whereas Z'' is normalized to its value at 0.01 Hz.

For Z'' [Fig. 6(a)], we observe that the plateau value around 10 Hz, as well as the larger values at low frequencies, scales inversely linear with light intensity since all curves coincide ($Z'I$ is constant), indicating they are indeed related to R_e via the electrical photoconduction. The decay at higher frequencies, governed by R_e and C_e , shifts linearly to larger frequencies with increasing light intensity due to the reduction in R_e . Similarly, in the normalized Z'' plot [Fig. 6(b)], the maximum at higher frequencies also shifts with frequency to higher frequencies with increasing light intensity, since this maximum is also governed by $1/R_e C_e$; since C_e has a constant value of $C_e = 1.6 \times 10^{-10}$ F, this shift is governed by the linear decrease in R_e with light intensity. We also observe that the low frequency part of the spectrum is light-intensity independent. This indicates that the time constant of the transient process does not depend on light intensity, as observed before.¹⁷ The time dependence of the transient electrical current then shows up as an apparent capacitance in the impedance spectra. In that case, the high capacitance of 10^{-6} F obtained from the fits under illumination is not related to charge or ion accumulation but is an artificial value resulting from a transient process with a fixed time constant. For increased light intensities, R_e decreases linearly with light intensity, such that C_{tr} needs to be adjusted in order to keep $R_e \times C_{tr}$ constant.

We also observe for every light intensity that the plateau value of Z' around 10 Hz has a value that is exactly half of the value of

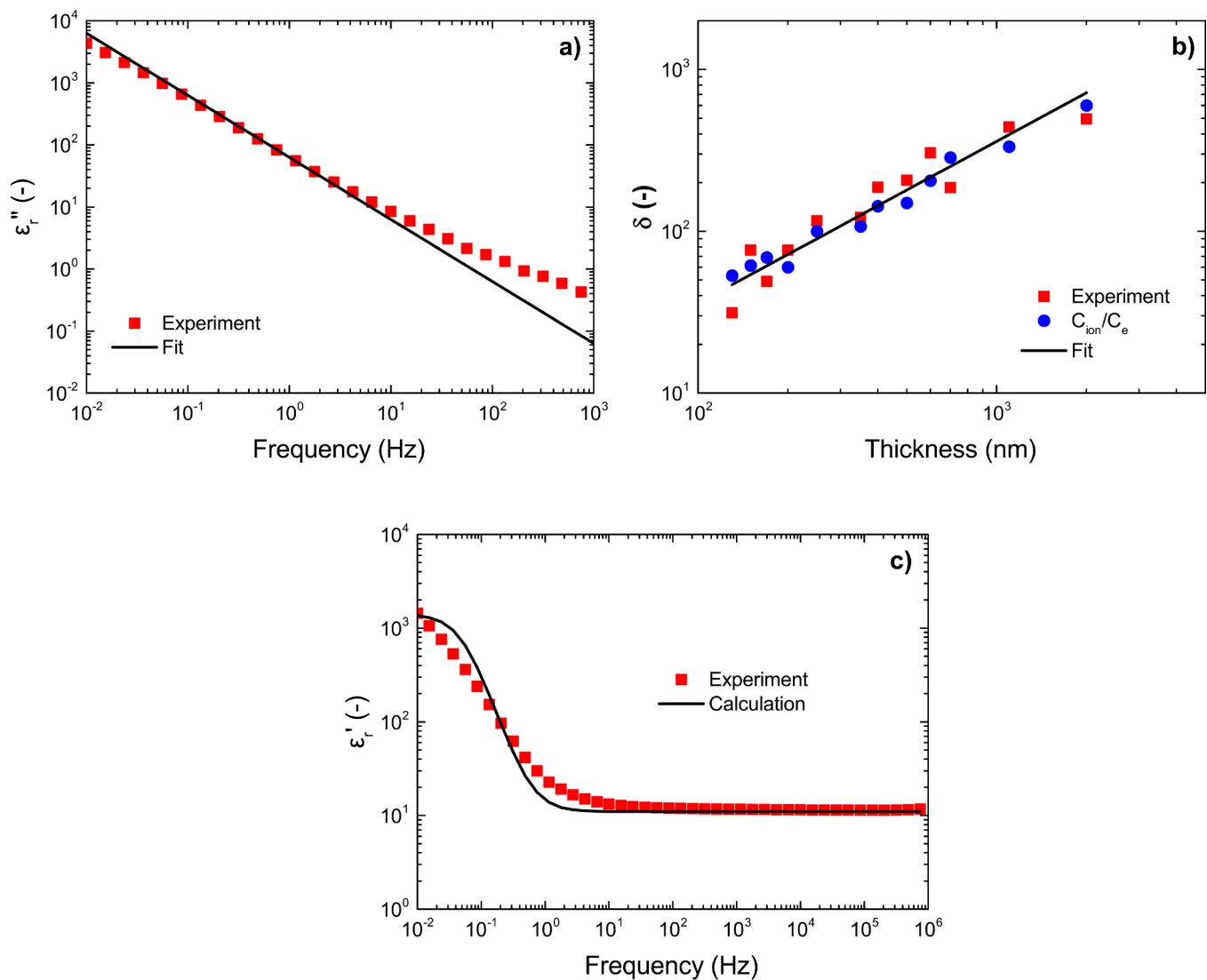


FIG. 5. (a) Dielectric loss ϵ_r'' as a function of frequency f for an Au/CsPbI₂Br/Au capacitor with a layer thickness L of 600 nm. The $1/f$ dependence of ϵ_r'' (Jonscher's law) is indicated by the solid line. (b) Parameter δ vs layer thickness obtained from the characteristic frequencies in Z'' (red symbols) as well as from the measured (blue symbols) and expected (line) capacitance ratio C_{ion}/C_e . (c) Effective dielectric constant ϵ_r' (symbols) as a function of frequency f for an Au/CsPbI₂Br/Au capacitor with a layer thickness d of 130 nm. The calculated frequency dependence of ϵ_r' [Eq. (3)] is given by the line, representing the polarization due to ions.

R_e . Due to the much lower values of R_e under illumination, the ionic branch is basically short-circuited by C_e at high frequencies (>100 Hz), by the branch with R_e and C_{tr} in series at intermediate frequencies (0.1–100 Hz) and by R_e at low frequencies (<0.01 Hz). For this reason, when using the extended circuit shown in the inset in Fig. 2(a) for the illuminated samples, the fits are insensitive for the ionic parameters. At the intermediate frequencies (0.1–100 Hz), the net impedance of the circuit is dominated by two branches: the branch with R_e and the branch with R_e and C_{tr} in series. The total impedance of R_e and C_{tr} in series is dominated by R_e , since in the

frequency range of 0.1–100 Hz, the impedance of $1/j\omega C_{tr}$ is still considerably smaller as compared to R_e . As a result, the total impedance of the circuit in the range of 0.1–100 Hz is governed by a parallel resistor of R_e in the two branches, which, in total, gives a resistance of $0.5R_e$. This then provides a logical explanation why under illumination at intermediate frequencies of ~ 10 Hz, the plateau value of Z' is exactly half of R_e .

This confirms the dominant role of the electrical resistance R_e in the transient current effect, validating the inclusion of R_e in the branch representing the transient effect. Furthermore, due to the

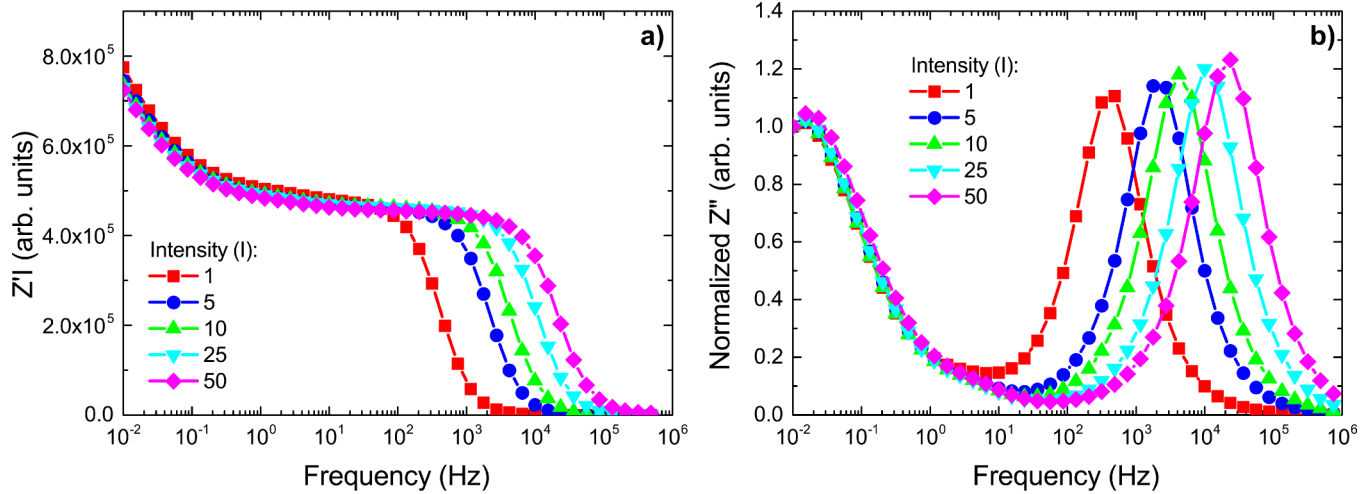


FIG. 6. (a) Real Z' multiplied by the light intensity I and (b) normalized imaginary part of the impedance Z''/Z' (0.01 Hz) as a function of frequency for an Au/CsPbI₂Br/Au capacitor with a thickness of 130 nm, illuminated with different relative light intensities of 1, 5, 10, 25, and 50.

insensitivity to the ionic parameters, an answer to the question whether the ion conduction changes under illumination cannot be obtained from the impedance spectra.

In earlier work, it was proposed that the transient effect in the electrical current/resistance originates from a change of the injection/extraction barrier due to the movement of ions.^{17,18} The independence of the time constant of the transient on light intensity basically rules out charge carriers as a source for this effect. The obtained ion diffusion coefficient $D_{ion} = 2 \times 10^{-17} \text{ m}^2/\text{s}$ corresponds to an ion mobility of $8 \times 10^{-16} \text{ m}^2/\text{s}$. Even for a 130 nm sample, the

transit time of an ion to cross the sample would amount to ~ 200 s for an applied voltage of 0.1 V, being three orders of magnitude larger than the observed time constant of 0.1 s. Furthermore, if such ion diffusion process would be the dominant source of the transient effect, a dependence of the characteristic time on sample thickness would be expected, which is not observed. From our analysis, we also obtained the thickness independent ionic capacitance C_{ion} of $3.5 \times 10^{-8} \text{ F}$, which corresponds to a Debye length of 3 nm. The time for an ion to move 3 nm inside the ion accumulation layer at 0.1 V amounts to 0.1 s, which is in agreement with the experimental value and is independent of the sample thickness. We, therefore, propose that the slow current transients leading to anomalous capacitances in the impedance originate from the reorganization of ions within the ion accumulation layer adjacent to the electrode under bias. This leads to the modification of the electric field at the interface, which, in turn, modulates the charge injection and extraction, leading to a transient current effect. This explanation is further strengthened by a decrease in the transient time constant with applied bias voltage V_{bias} , as shown in Fig. 7, using capacitors with varying thickness. Such a decrease would be expected for a time constant governed by the drift of an ion in an applied electric field. A more quantitative analysis would require the exact spatial electric field distribution in the film, which is beyond the scope of this paper.

Understanding of the various contributions to the experimental dielectric properties of perovskite capacitors lays the foundation for the device models of perovskite devices as solar cells and LEDs.

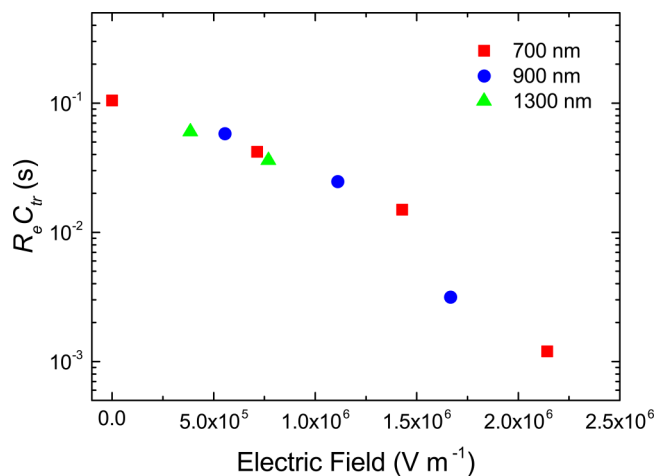


FIG. 7. Transient time constant $R_e \times C_{tr}$ as a function of the applied electric field for Au/CsPbI₂Br/Au capacitors with a thickness of 700, 900, and 1300 nm, respectively.

III. CONCLUSIONS

In conclusion, we have analyzed the impedance spectra of perovskite capacitors to disentangle the processes of charge and ion movement in the dark. The impedance data of perovskite-based capacitors in the dark are well described using an extended

Maxwell circuit including a branch with a fixed time constant of ~ 0.1 s. From the thickness dependence of the electrical and ionic resistance, the electrical and ionic conductivities can be obtained. The dominance of ionic conduction allows for a quantitative analysis of the impedance spectra to reveal the ion dynamics. It is demonstrated that the characteristic frequencies of the spectra are directly correlated with the formation of an ionic space-charge layer. Compared to MAPbI₃, the ion diffusion coefficient in CsPbI₂Br is about two orders of magnitude lower, making the impedance data at low frequencies less sensitive to ion motion. The impedance spectra under illumination are dominated by the strongly reduced electrical resistance as a result of photoconduction. As a mechanism for the current transient, we propose the spatial reorganization of ions within the ionic space-charge layer.

IV. EXPERIMENTAL SECTION

A. Device fabrication

Cr(1 nm)/Au(18 nm) was deposited as the bottom electrode on a glass substrate by thermal evaporation in high vacuum. A mixture of 0.72 M PbI₂, 0.72 M PbBr₂, and 1.44 M CsI in DMSO was prepared, filtered, and then spin coated on the substrate inside a glovebox under an N₂ atmosphere. Finally, a 60 nm Au layer was deposited on top of perovskite films to form capacitors with a device area of 1 mm².

B. Thickness of the perovskite layer

The spin coating was performed at 500 rpm for 3 s, followed by 2000 rpm for 30 s. After repeating the process three times, the films were annealed at 40 °C until turning red at the surface and then further annealed at 160 °C for 10 min. A perovskite film with a thickness of 600 nm could be formed with this procedure. For different thicknesses, the speed of the second spin coating step was adapted accordingly from 500 to 4000 rpm.

C. Device characterization

Impedance measurements were conducted in a nitrogen-filled glovebox, using a high-performance frequency analyzer, Novocontrol, Alpha-A. The samples were illuminated with a white light-emitting diode from a Paios system from Fluxim AG, with a maximum light intensity equivalent to approximately 1 Sun.

SUPPLEMENTARY MATERIAL

See the [supplementary material](#) for a derivation of the frequency of the minimum in Z'' as well as a statistical analysis including a figure showing the impact of the change of the electrical resistance on the impedance spectrum.

AUTHOR DECLARATIONS

Conflict of Interest

The authors have no conflicts to disclose.

Author Contributions

Cong Xu: Data curation (lead); Formal analysis (equal); Investigation (lead); Validation (equal); Writing – original draft (equal). **Mohammad Sajedi Alvar:** Formal analysis (supporting); Investigation (supporting); Software (lead). **Gert-Jan A. H. Wetzelaer:** Formal analysis (supporting); Investigation (supporting); Supervision (equal); Validation (equal); Writing – original draft (equal). **Paul W. M. Blom:** Conceptualization (equal); Formal analysis (lead); Methodology (equal); Supervision (equal); Validation (lead); Writing – original draft (equal).

DATA AVAILABILITY

The data that support the findings of this study are available from the corresponding author upon reasonable request.

REFERENCES

- ¹H. J. Snaith, *J. Phys. Chem. Lett.* **4**, 3623–3630 (2013).
- ²Z.-K. Tan, R. Saberi Moghaddam, M. L. Lai, P. Docampo, R. Higler, F. Deschler, M. Price, A. Sadhanala, L. M. Pazos, D. Credgington, F. Hanusch, T. Bein, H. J. Snaith, and R. H. Friend, *Nat. Nanotechnol.* **9**, 687–692 (2014).
- ³B. Chen, M. Yang, S. Priya, and K. Zhu, *J. Phys. Chem. Lett.* **7**, 905–917 (2016).
- ⁴S. van Reenen, M. Kemerink, and H. J. Snaith, *J. Phys. Chem. Lett.* **6**, 3808–3814 (2015).
- ⁵J. Haruyama, K. Sodeyama, L. Han, and Y. Tateyama, *J. Am. Chem. Soc.* **137**, 10048–10051 (2015).
- ⁶A. Sawada, *J. Chem. Phys.* **129**, 064701 (2008).
- ⁷J. R. MacDonald, *Impedance Spectroscopy* (John Wiley & Sons, New York, 1987).
- ⁸M. Sajedi Alvar, P. W. Blom, and G. J. A. H. Wetzelaer, *Adv. Electron. Mater.* **6**, 1900935 (2020).
- ⁹T. M. W. J. Bandara and B.-E. Mellander, in *Ionic Liquids Theory, Properties, New Approaches*, edited by A. Kokorin (InTech, 2011), Chap. 17.
- ¹⁰J. Beilstein-Edmands, G. E. Eperon, R. D. Johnson, H. J. Snaith, and P. G. Radaelli, *Appl. Phys. Lett.* **106**, 173502 (2015).
- ¹¹E. J. Juarez-Perez, R. S. Sanchez, L. Badia, G. Garcia-Belmonte, Y. S. Kang, I. Mora-Sero, and J. Bisquert, *J. Phys. Chem. Lett.* **5**, 2390–2394 (2014).
- ¹²A. Dualeh, T. Moehl, N. Tétreault, J. Teuscher, P. Gao, M. K. Nazeeruddin, and M. Grätzel, *ACS Nano* **8**, 362 (2014).
- ¹³I. Zarazua, J. Bisquert, and G. Garcia-Belmonte, *J. Phys. Chem. Lett.* **7**, 525 (2016).
- ¹⁴A. Zohar, N. Kedem, I. Levine, D. Zohar, A. Vilan, D. Ehre, G. Hodes, and D. Cahen, *J. Phys. Chem. Lett.* **7**, 191 (2016).
- ¹⁵A. Pockett, G. E. Eperon, N. Sakai, H. J. Snaith, L. M. Peter, and P. J. Cameron, *Phys. Chem. Chem. Phys.* **19**, 5959 (2017).
- ¹⁶D. Moia, I. Gelmetti, P. Calado, W. Fisher, M. Stringer, O. Game, Y. Hu, P. Docampo, D. Lidzey, E. Palomares, J. Nelson and P. R. F. Barnes, *Energy Environ. Sci.* **12**, 1296–1308 (2019).
- ¹⁷F. Ebadi, N. Taghavinia, R. Mohammadpour, A. Hagfeldt, and W. Tress, *Nat. Commun.* **10**, 1574 (2019).
- ¹⁸W. Choi, S. W. Song, S. G. Han, and K. Cho, *Adv. Electr. Mater.* **6**, 2000030 (2020).
- ¹⁹W. Zhou, Y. Zhao, X. Zhou, R. Fu, Q. Li, Y. Zhao, K. Liu, D. Yu, and Q. Zhao, *J. Phys. Chem. Lett.* **8**, 4122 (2017).
- ²⁰S. M. Yoon, H. Min, J. B. Kim, G. Kim, K. S. Lee, and S. I. Seok, *Joule* **5**, 183–196 (2021).
- ²¹S. Ullah, J. Wang, P. Yang, L. Liu, Y. Li, S.-E. Yang, T. Xia, H. Guo, and Y. Chen, *Energy Technol.* **9**, 2100691 (2021).
- ²²A. Jonscher, *J. Mater. Sci.* **13**, 553–562 (1978).